




Mini-review on self-interacting dark matter

Manoranjan Dutta^{1,a}  and Satyabrata Mahapatra^{2,b}

¹ Department of Physics, North Lakhimpur University, Khelmati, Lakhimpur 787031, Assam, India

² Department of Physics and Institute of Basic Science, Sungkyunkwan University, Suwon 16419, South Korea

Received 29 August 2023 / Accepted 14 February 2024

© The Author(s), under exclusive licence to EDP Sciences, Springer-Verlag GmbH Germany, part of Springer Nature 2024

Abstract In this mini-review, we explore an alternative paradigm to cold dark matter (CDM) postulated in Λ CDM model. The alternative known as the self-interacting dark matter (SIDM) addresses inconsistencies of Λ CDM predictions at small scales, the most prominent one being the *cusp-core problem*. We delve into the particle physics aspect of SIDM model building, focusing on SIDM via light mediators. However, light mediator models face challenges with thermal relic abundance due to efficient annihilation of SIDM and constraints from direct search, Big Bang Nucleosynthesis etc.. We then discuss two specific SIDM set-ups incorporating tiny neutrino masses. The first one involves a right-handed neutrino portal adjusting for relic deficit through its late decay. This portal connects the dark sector to neutrino mass and is realized in two UV complete ways—scotogenic and gauged B – L. The second set-up features a singlet–doublet extended model, where doublet becomes long-lived, thanks to extremely small singlet–doublet mixing. The late decay of the doublet contributes non-thermally to the singlet SIDM relic. Adding a scalar doublet and two singlet fermions, which are odd under a Z_2 symmetry, we also address eV-scale mass of neutrinos generated by a scotogenic set-up. In both scenarios, we explore the parameter space that leads to sufficient self-interaction and correct relic density. Our analysis incorporates all pertinent astrophysical, cosmological, experimental, and phenomenological constraints.

1 Introduction

Dark matter is hypothesized as a form of matter which does not interact with radiation. Its existence is evident from its gravitational effects, such as the rotational velocities of stars, gravitational lensing, anisotropies in cosmic microwave background (CMB) *etc.* According to latest results from WMAP [1] and Planck [2] experiments, it contributes one fifth of energy budget of the cosmos. Despite its prevalence, the Standard Model (SM) falls short for a suitable DM candidate. Among many possibilities beyond the SM, weakly interacting massive particles (WIMPs) have long enjoyed the limelight. WIMP explains the observed relic density through ‘*thermal freeze-out*’ from hot cosmic soup. WIMP has mass and couplings at the weak scale. Its interactions with the visible sector might be sufficient to detect it in terrestrial direct search laboratories. However, direct detection experiments so far have not found any conclusive evidence of DM. This casts serious doubt over the minimal WIMP setups. Completed and ongoing direct search experiments rule out typical WIMPs up to a few TeVs after probing DM–nucleon cross-section down to 10^{-47}cm^2 [3–5]. Moreover, the non-observation of missing energy signatures at LHC put severe constraints on minimal WIMP-like DM models.

From a cosmological perspective, the most widely accepted model for the universe *i.e.*, the Λ CDM model, incorporates DM as non-relativistic and collisionless fluid, that played a crucial role in the formation of structures in the early universe. The agreement of predictions of the Λ CDM model with observed CMB angular power spectrum provides strong evidence for CDM. Predictions of Λ CDM also align well with large-scale structures of the universe. On astrophysical scales, typical WIMP interactions are negligible, making them well-suited for the cold and collisionless DM assumed in the Λ CDM model.

Manoranjan Dutta and Satyabrata Mahapatra contributed equally to this manuscript.

^a e-mail: dutta.manoranjan@nlc.ac.in (corresponding author)

^b e-mail: satyabrata@g.skku.edu

However, of late, improved cosmological N-body simulations [6, 7], have revealed some serious discrepancies of Λ CDM with astrophysical observations. While Λ CDM successfully explains large-scale structures, it tends to over-predict the rotation speed of stars (and hence the amount of DM enclosed) at small scales. The discrepancies include the ‘*cusp-core problem*’ related to halo density profiles in galaxies [8, 9], the ‘*missing-satellite problem*’ that involves the over-prediction of small satellite galaxies in Λ CDM simulations [10, 11] and the ‘*too big to fail problem*’ associated with the absence of the most luminous satellite galaxies in the most massive sub-halos [12, 13]. To alleviate these anomalies, self-interacting dark matter (SIDM) was proposed in 2000 [14] (See for earlier studies [15, 16]). Unlike CDM, SIDM has very large self-scattering among themselves, often quantified as $\sigma/M_{DM} \sim \mathcal{O}(10^{-24} \text{ cm}^2/\text{GeV})$. This is fourteen orders of magnitude larger compared to the scale of WIMP cross-section $\sigma/M_{DM} \sim \mathcal{O}(10^{-38} \text{ cm}^2/\text{GeV})$. Self-interaction scatters DM particles out of the dense halo centres, remarkably affecting dwarf and galactic size dynamics by particle interaction. However, at the cluster scale and beyond [17], success of Λ CDM constrains SIDM. Hence, preferred cross-section is highest at the scale of dwarf galaxies and gradually decreases towards cluster scales [18, 19]. Self-interaction cross-section with a desired dependence on collision velocities can potentially alleviate these problems by primarily affecting small-scale dynamics. At the same time, SIDM predictions remain consistent with those of Λ CDM at large scales.

The issues of Λ CDM in small scale and lack of direct WIMP detection make it motivating to explore alternative scenarios for DM. Light DM which exhibits significant self-scattering while being elusive to direct detection is particularly intriguing. Theoretical models that can simultaneously account for both DM and neutrino mass are highly desirable as they necessitate addressing constraints from relevant phenomenologies and experiments in both sectors. These models provide more complementary probes compared to their individual counterparts, benefiting from the availability of a wider range of experimental tests. In this review, we explore SIDM phenomenologies from particle physics point of view, followed by a few model-building approaches that simultaneously address both SIDM and neutrino phenomenology.

This review is organised with the following sections. In Sect. 2, we explore how SIDM alleviates the small-scale anomalies as well as constraints on SIDM from large-scale structures of the universe. In Sect. 3, we delve into model-building approaches for SIDM from a particle physics perspective with special attention to light mediator based models. Then, we go on to discuss two specific works based on [20, 21]. In Sect. 4, we discuss the SIDM via right-handed neutrino portal and in sec. 5, we discuss a SIDM scenario based on singlet–doublet extension of the SM. We then conclude in Sect. 6.

2 SIDM and small-scale anomalies of Λ CDM

SIDM introduces notable properties to the DM halos compared to CDM, such as isothermal velocity dispersion, reduced central density etc. [18]. Self-scattering redistributes heat to the inner halo from the outer halo, resulting in a uniform velocity dispersion across different radii. Through scattering, particles in dense inner halo gain energy and are scattered away from the central region, transforming the cuspy density profile (where density decreases as the inverse of the radius) into a cored profile (where density remains roughly constant with radius). The rate of scattering is directly proportional to DM density. Therefore, it has the maximum impact near the center of halos. The rate of collision becomes negligible at sufficiently large scale, and the halo properties match those of CDM. Hence, SIDM retains Λ CDM’s success in explaining the cosmos at large scale. It mainly affects the small-scale structures formed at late times within the dense inner halo. The local collision rate (R) of SIDM can be approximated as [18],

$$R = \sigma v_{\text{rel}} \rho_{\text{DM}} / M_{DM} \approx 0.1 \text{ Gyr}^{-1} \times \left(\frac{\rho_{\text{DM}}}{0.1 \text{ M}_{\odot}/\text{pc}^3} \right) \left(\frac{v_{\text{rel}}}{10 \text{ km/s}} \right) \left(\frac{\sigma/M_{DM}}{1 \text{ cm}^2/\text{g}} \right). \quad (1)$$

Here, σ denotes cross-section for self-interaction, v_{rel} denotes the relative collision velocity, ρ_{DM} and M_{DM} are, respectively, the local density of DM and DM mass. For alleviating the small-scale anomalies, DM self-interaction must be active at much later epochs (after galaxy formation).¹ In this context, the collision velocity is of the scale of escape velocities of the concerned astrophysical objects. This leads to significant differences in the magnitude of scattering cross-sections for dwarfs, galaxies, and clusters, as each of these objects is characterized by distinct escape velocity scales. For the central halo of dwarf galaxies, $\rho_{\text{DM}} \sim 0.1 \text{ M}_{\odot}/\text{pc}^3$, $v_{\text{rel}} \sim 10 \text{ km/s}$ [22]. Therefore, we can approximate [23–28],

$$\sigma/M_{DM} \sim 1 \text{ cm}^2/\text{g} \approx 1 \times 10^{-24} \text{ cm}^2/\text{GeV}. \quad (2)$$

¹Though self scattering might be there before structure formation, but it falls out of equilibrium very rapidly due to expansion of the universe and red-shift. Therefore, if σ/M_{DM} is not too much larger than $1 \times 10^{-24} \text{ cm}^2/\text{GeV}$, the scattering rate R is negligible at the epoch of structure formation.

This corresponds to roughly one scattering per particle per 10 Gyr galactic time-scales [18]. The typical mean free path is larger than the core radii facilitating heat conduction effectively in the inner halo. CDM-only simulations described by the NFW profile [6, 29, 30] gives a cuspy DM density profile. In this case, $\rho_{DM} \propto r^{-1}$ in the inner halo. But as per observations, rotation curves of many dwarf galaxies rise linearly with radius $v(r) \propto r$ [31, 32], which is possible only if the central halo is a constant density core *i.e.*, $\rho(r) \propto r^0$. This is essentially the ‘*cusps-core problem*’, most prominent in dwarfs and LSB galaxies [8, 33–44]. It was shown in [45, 46] that cored profiles better fits the data from dwarf galaxy DDO 154. It is assumed that a demarcation between the outer and inner halo is established at a radius r_1 , where, there is on average, one collision per particle throughout the age of the halo ($t_{\text{age}} \sim 5 - 10$ Gyr). The density profile ρ_{DM} is given by:

$$\rho_{DM}(r) = \begin{cases} \rho_{\text{iso}}(r), & r < r_1 ; \\ \rho_{\text{NFW}}(r), & r > r_1 ; \end{cases} \tag{3}$$

where, ρ_{iso} and ρ_{NFW} are the isothermal and NFW density profile, respectively.

The isothermal profile within the inner $r < r_1$ region is expected to originate from the self-interaction among DM particles which thermalizes their distribution, while the outer region ($r > r_1$) is given by the usual NFW profile for collisionless CDM. At $r = r_1$, results from both sides are to be matched.

Similarly, the suppression of the subhalo mass function on the scale of galaxies is relevant in addressing the issue of the *missing satellites* [10, 11]. SIDM, owing to reduced central density profiles also address the *too-big-to-fail* problem [12, 13, 27, 28].

Astrophysical observations impose various constraints on the SIDM paradigm, primarily driven by the remarkable success of Λ CDM in explaining the universe at large scale. A stringent constraint of $\sigma/M_{DM} \leq 0.1 \text{ cm}^2/\text{g}$ [47, 48] is obtained from strong lensing and central density measurements of the MS2137-23 cluster yield. A slightly weaker constraint of $\sigma/M_{DM} \lesssim 1 \text{ cm}^2/\text{g}$ comes from the Bullet Cluster [17]. Numerical studies of DM-galaxy offset indicate that the self-interaction is highest at the dwarf galaxy scale and gradually decreases towards larger scales, with strong self-interactions being excluded beyond the cluster scale [49–54]. The consensus emerging from these studies is that the range of $\sigma/M_{DM} \sim 0.5 - 1 \text{ cm}^2/\text{g}$ is sufficient to ameliorate the ‘*cusps-core problem*’ and the ‘*too-big-to-fail problem*’ at small scales, which leaves large scale structures undisturbed. [27, 53–55].

3 Particle physics aspects of SIDM

Very early attempts to realize large σ/M_{DM} includes postulating a real scalar field ϕ as DM [56, 57], where self-interaction may arise via quartic term $\mathcal{L} = -\frac{\lambda}{4!}\phi^4$. This, however, yields a velocity-independent self-scattering cross-section $\sigma(\phi\phi \rightarrow \phi\phi) = \lambda^2/(128\pi m_\phi^2)$, which is undesired. Instead, a cross-section with dependence on collision velocity (similar to n-p scattering mediated by pions) is better suited which remains aligned with large scale Λ CDM predictions. However, unlike nucleon scattering, self-interactions can be weakly coupled with a light mediator [19, 23–26, 58, 59]. For a SIDM (mediator) of mass M_{DM} (M_{med}), in the limit $\alpha_D M_{DM}/M_{med} \ll 1$ and $v_{\text{rel}} = 0$, perturbative calculation yields,

$$\sigma/M_{DM} = \frac{4\pi\alpha_D^2 M_{DM}}{M_{med}^4} \approx 1 \text{ cm}^2/\text{g} \times \left(\frac{\alpha_D}{0.01}\right)^2 \left(\frac{M_{DM}}{10 \text{ GeV}}\right) \left(\frac{M_{med}}{40 \text{ MeV}}\right)^{-4}; \tag{4}$$

where $\alpha_D = \frac{g_D^2}{4\pi}$, g_D being the dark coupling constant. Provided the mediator is light enough ($M_{med} \ll M_{DM}$), DM of weak scale mass and self-interactions of the order of electromagnetic strength are at the necessary ballpark to obtain sufficient self-interaction with desired velocity dependence. It is noteworthy that Eq. (4) holds good in the perturbative regime ($\alpha_D M_{DM}/M_{med} \ll 1$) only and does not hold good beyond this approximation. Here, we note that, though strongly interacting massive particle (SIMP) models [15, 60–62] do introduce a form of self-interaction, they may not inherently yield the same velocity-dependent features as SIDM scenarios we discuss here. SIMP models often involve complex dynamics within a non-Abelian dark sector, leading to strong interactions but potentially lacking the explicit velocity-dependent behavior associated with light mediator exchanges in SIDM. The specific characteristics are model dependent. Some specific models with self-heating SIMPs may have the necessary velocity dependence to avoid bounds from observations at cluster scales [63–65].

In the next sub-section, we discuss light mediator based SIDM models producing desired self-interaction within as well as beyond the perturbative regime.

3.1 SIDM with light mediators

Sufficiently large self-interactions is readily realised via SIDM models with light mediators (below the GeV scale). These models also possess the desired velocity dependence. Such light mediators can be realised easily in BSM models extended by scalar or vector boson mediators [19, 23–26, 45, 59, 66–69]. Spontaneously broken $U(1)$ models are well suited for such a scenario, where the stability of DM is assured due to charge conservation. The generic interaction Lagrangian for such models assuming the SIDM as a Dirac fermion ψ can be given by:

$$\mathcal{L}_{\text{int}} = \begin{cases} g_D \bar{\psi} \gamma^\mu \psi X_\mu & (\text{vector mediator}) \\ g_D \bar{\psi} \psi X & (\text{scalar mediator}). \end{cases} \quad (5)$$

Here, g_D is dark coupling constant and X_μ (X) is vector (scalar) mediator. A representative feynman graph for self scattering is presented in the left panel of Fig. 1.

In the non-relativistic limit, the scattering is well-described in terms of a Yukawa-type potential,

$$V(r) = \pm \frac{\alpha_D}{r} e^{-M_X r}; \quad (6)$$

where $\alpha_D = \frac{g_D^2}{4\pi}$. For vector mediator, $\psi\bar{\psi}$ scattering leads to a attractive ($-$) potential, while $\psi\psi$ or $\bar{\psi}\bar{\psi}$ scattering leads to a repulsive ($+$) potential. For scalar mediated case, the potential is always attractive. In perturbative regime ($\alpha_D M_{DM}/M_X \ll 1$), differential cross-section is,

$$\frac{d\sigma}{d\Omega} = \frac{\alpha_D^2 M_{DM}^2}{[M_{DM}^2 v_{\text{rel}}^2 (1 - \cos\theta)/2 + M_X^2]^2}. \quad (7)$$

In the limit $M_X \gg M_{DM} v_{\text{rel}}$, it behaves like contact interaction. In this limit, scattering cross-section does not depend on v_{rel} . Contrarily, when $M_X \ll M_{DM} v_{\text{rel}}$, cross-section goes as $1/v_{\text{rel}}^4$ similar to Rutherford scattering [25, 58, 70]. Neither of these two limits provide the desired mild velocity-dependence [45]. But a small yet non-zero mediator mass provides the correct velocity-dependence. This necessitates a transition from contact to Rutherford scattering roughly at $v_{\text{rel}} \approx 300$ km/s, which falls in midway of dwarf and cluster velocities. This implies $M_X/M_{DM} \sim v_{\text{rel}}/c \sim 10^{-3}$. This can be satisfied by $M_{DM} \sim \mathcal{O}(10 \text{ GeV})$ with the mediator mass $M_X \sim \mathcal{O}(10 \text{ MeV})$. To encompass the pertinent aspects of forward scattering in self-interaction, we define the transfer cross-section (σ_T) as [18, 19, 24]:

$$\sigma_T = \int d\Omega (1 - \cos\theta) \frac{d\sigma}{d\Omega}. \quad (8)$$

In perturbative regime ($\alpha_D M_{DM}/M_X \ll 1$), σ_T is obtained by integrating the differential cross-section given in Eqn. 7, which gives

$$\sigma_T^{\text{Born}} = \frac{8\pi\alpha_D^2}{M_{DM}^2 v^4} \left(\ln(1 + M_{DM}^2 v^2/M_X^2) - \frac{M_{DM}^2 v^2}{M_X^2 + M_{DM}^2 v^2} \right). \quad (9)$$

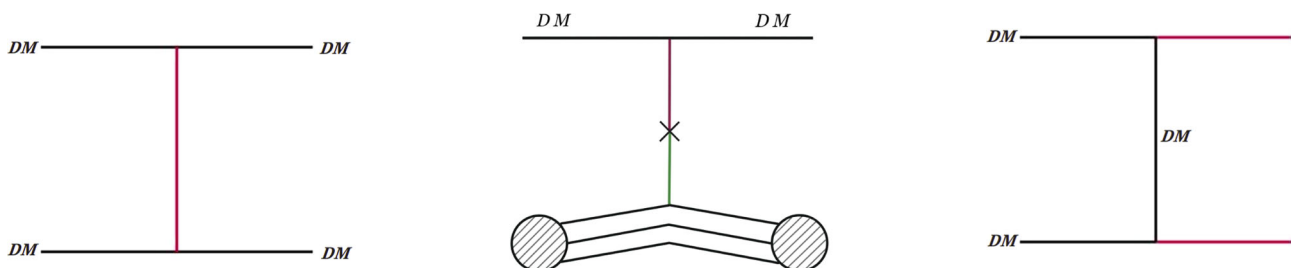


Fig. 1 Representative Feynman graphs for self scattering (left), SIDM direct detection (centre) and SIDM freeze-out (right). The black, red and green lines represents SIDM (ψ), light BSM mediator (X_μ or X) and some SM mediator respectively. The specific properties of these particles depend on the choice of model

Outside the perturbative regime ($\alpha_D M_{DM}/M_X \geq 1$), we get a pair of distinct regimes. For classical regime ($\alpha_D M_{DM}/M_X \geq 1, M_{DM}v/M_X \geq 1$), the solutions are is given by[19, 24, 59, 71, 72],

$$\sigma_T^{\text{classical}}(\text{Attractive}) = \begin{cases} \frac{4\pi}{M_X^2} \beta^2 \ln(1 + \beta^{-1}) & \beta \leq 10^{-1} \\ \frac{8\pi}{M_X^2} \beta^2 / (1 + 1.5\beta^{1.65}) & 10^{-1} \leq \beta \leq 10^3 \\ \frac{\pi}{M_X^2} (\ln \beta + 1 - \frac{1}{2} \ln^{-1} \beta) & \beta \geq 10^3; \end{cases} \tag{10}$$

$$\sigma_T^{\text{classical}}(\text{Repulsive}) = \begin{cases} \frac{2\pi}{M_X^2} \beta^2 \ln(1 + \beta^{-2}) & \beta \leq 1 \\ \frac{\pi}{M_X^2} (\ln 2\beta^2 - \ln \ln 2\beta)^2 & \beta \geq 1; \end{cases} \tag{11}$$

where $\beta = 2\alpha_D M_X / (M_{DM}v^2)$. For $\alpha_D M_{DM}/M_X \geq 1, M_{DM}v/M_X \leq 1$, we get the resonant regime. In this regime, σ_T has the distinct feature of resonances and anti-resonances. The resonances occur due to formation of (quasi)-bound states in the potential. Of course, this occurs only for the attractive potential. As no bound state forms in the repulsive potential, hence no resonance appears in that case. It is not possible to obtain an analytical formula for the resonant regime. Here, we employ non-perturbative results obtained by approximating the Yukawa potential as Hulthen potential ($V(r) = \pm \frac{\alpha_D \delta e^{-\delta r}}{1 - e^{-\delta r}}$) given by [19]:

$$\sigma_T^{\text{Hulthen}} = \frac{16\pi \sin^2 \delta_0}{M_{DM}^2 v^2}; \tag{12}$$

where δ_0 , the phase shift for $l = 0$ is given by:

$$\delta_0 = \arg\left(\frac{i\Gamma\left(\frac{iM_{DM}v}{kM_X}\right)}{\Gamma(\lambda_+)\Gamma(\lambda_-)}\right), \quad \lambda_{\pm} = \begin{cases} 1 + \frac{iM_{DM}v}{2kM_X} \pm \sqrt{\frac{\alpha_D M_{DM}}{kM_X} - \frac{M_{DM}^2 v^2}{4k^2 M_X^2}} & \text{Attractive} \\ 1 + \frac{iM_{DM}v}{2kM_X} \pm i\sqrt{\frac{\alpha_D M_{DM}}{kM_X} + \frac{M_{DM}^2 v^2}{4k^2 M_X^2}} & \text{Repulsive.} \end{cases} \tag{13}$$

Here, Γ is Gamma function and $k \approx 1.6$ is a dimensionless number obtained by matching the results from the Hulthen potential with Born cross-section in $v \rightarrow 0$ limit. The important feature of the resonant regime is the non-trivial velocity dependence. At resonance, the phase shift $|\delta_0| \rightarrow 0$ for $v \rightarrow 0$, and $\sigma_T \sim \frac{16\pi}{M_{DM}v^2}$. At very high velocities, all these cross-sections converge to the Coulomb result $\sigma_T M_{DM}^2 \propto \frac{1}{v^4}$ irrespective of the ratio M_X/M_{DM} . By employing these cross-sections, we explore the parameter space allowed for self-interaction in terms of M_{DM} and M_X , consistent with observational data from astrophysical sources across various scales. The permitted parameter space is illustrated in Fig. 2, where σ/M_{DM} is constrained within the range of $0.1 - 10 \text{cm}^2/\text{g}$ for galaxies and dwarfs. The allowed regions are depicted by shades of cyan and green, respectively. The corresponding region for clusters ($\sigma/M_{DM} \sim 0.1 - 1 \text{cm}^2/\text{g}$) is shown in light magenta color. DM and mediator mass range for which all regions overlap is suitable for addressing the small-scale problems at all scales.

We expect dark sector not to be entirely secluded. Instead, we expect some coupling of the light mediator with SM particles, bringing both sectors into thermal equilibrium in the early cosmos. If the coupling is not strong enough, it may result in DM production in a non-thermal way. The same portal also enables its direct detection in terrestrial laboratories, as represented by the Feynman graph in the centre segment of Fig. 1. Due to sizeable gauge coupling, DM has a very large annihilation cross-section into the light mediators. For example, the most dominant process in determining SIDM relic is the t-channel process $DM DM \rightarrow XX$ (represented by Feynman graph in right segment of Fig. 1), for which the thermally averaged cross-section is approximated as,

$$\langle \sigma v \rangle \sim \frac{\pi \alpha_D^2}{M_{DM}^2} \left(1 - \frac{M_X^2}{M_{DM}^2}\right)^{\frac{1}{2}}; \tag{14}$$

where $\alpha_D = g_D^2/(4\pi)$. For $g_D \sim 0.1, M_{DM} \sim 1 \text{ GeV}$ and $M_X \sim 0.01 \text{ GeV}$, $\langle \sigma v \rangle$ is larger than that for typical WIMPs roughly by two orders of magnitudes. We define the dimensionless parameter $x = M_{DM}/T$ and $Y_{DM} = n_{DM}/s(T)$ where $s(T) = \frac{2\pi^2}{45} g_* S T^3$ is the entropy density of the universe. The evolution of co-moving DM number density Y_{DM} is obtained by the Boltzmann equation,

$$\frac{dY_{DM}}{dx} = -\frac{s(M_{DM})}{x^2 H(M_{DM})} \langle \sigma v \rangle (Y_{DM}^2 - (Y_{DM}^{eq})^2). \tag{15}$$

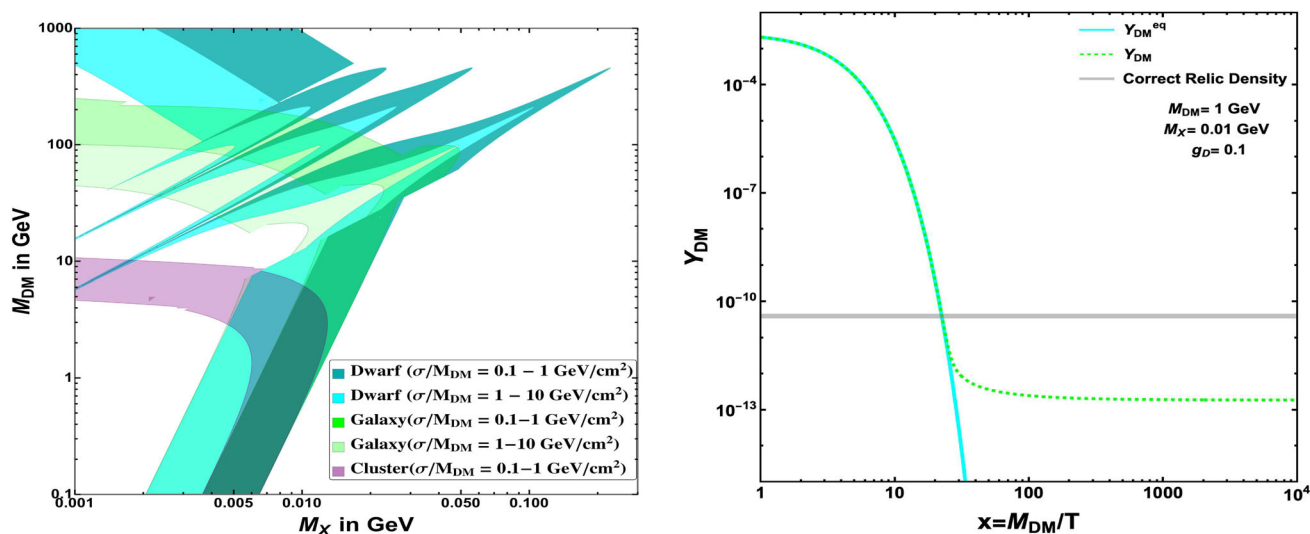


Fig. 2 [Left]: σ/M_{DM} in different ranges for clusters ($v \sim 1000 \text{ km/s}$), galaxies ($v \sim 100 \text{ km/s}$) and dwarfs ($v \sim 10 \text{ km/s}$). [Right]: Freeze out abundance of SIDM

The under-abundant relic obtained from standard freeze-out using Eq. 15 is shown in the right segment of Fig. 2.

Coupling between the two sectors faces severe constraints from terrestrial DM search experiments [73, 74]. The same mixing makes the mediator unstable against its decay to SM states and hence, early universe physics like Big Bang Nucleosynthesis (BBN) [2, 75–77] puts a lower bound on the mixing as such decays must occur before the onset of BBN to keep BBN predictions intact. The mass and mixing of the mediator being sandwiched between direct search and BBN bounds, and DM to mediator mass ratio being constrained from the requirement of sufficient self-interactions, SIDM models have a pretty concrete range of viable parameter space. Several efforts have been made in this direction [20, 21, 78–88]. In the subsequent sections, we briefly discuss two such SIDM scenarios in connection with the neutrino mass presented in [20, 21].

4 SIDM via right-handed neutrino portal

To address the challenge of the insufficient relic density of SIDM and to accommodate the small but confirmed non-zero neutrino mass, we delve into an $U(1)$ extension of the SM. Within this framework, a RHN introduced for neutrino mass generation, assumes a dual role by contributing to non-thermal SIDM production at a later epoch. In this set up, a fermion singlet carrying $U(1)_D$ charge is proposed as the DM candidate. Self-scattering is mediated by the $U(1)_D$ gauge boson (Z'). Achieving the desired SIDM phenomenology necessitates Z' being substantially lighter than the DM, with a significant gauge coupling. This coupling, however, leads to under-abundance of thermal SIDM relic due to increased annihilation into Z' , as detailed in Sect. 3. To surmount this challenge, we introduce a minute kinetic mixing of $U(1)_D$ with $U(1)_Y$, facilitating production of DM through freeze-in. This inclusion of a small kinetic mixing is also driven by the need to circumvent stringent direct search constraints. Notwithstanding these adjustments, the relic density of DM remains insufficient due to efficient annihilation of DM into Z' pairs. To address this, we introduce additional DM production mechanisms through late decay of one of the RHNs. This study particularly explores the scenario where the lightest RHN produced thermally from the cosmic plasma freezes out, and subsequently converts its abundance into SIDM through late-stage decay. This framework establishes a linkage between RHNs, neutrino masses, and SIDM. We delve into different seesaw models, such as gauged $B - L$, scotogenic etc., showcasing their ability to generate the desired relic of the lightest RHN. We constrain model parameters by ensuring desired relic density of the lightest RHN, to be transferred later to the SIDM abundance. We also discuss its implications concerning LHC and charged lepton flavor violation (CLFV). Additionally, we explore implications for astrophysical observations and the direct detection of SIDM.

4.1 Minimal setup

The minimal model is essentially an extension of the SM with an additional $U(1)_D$ symmetry. This symmetry entails a singlet Dirac fermion χ with non-zero charge as the SIDM candidate [20]. Another singlet scalar field (Φ)

carrying identical charge as χ and RHN N_R uncharged under $U(1)_D$ imparts the model with a generic Lagrangian:

$$\begin{aligned} \mathcal{L}_{Model} = & \mathcal{L}_{SM} + i\bar{\chi} \gamma^\mu (\partial_\mu - ig_D Z'_\mu) \chi - m_\chi \bar{\chi} \chi - \frac{1}{2} M_{N_R} \bar{N}^c N_R - y\chi\Phi N_R - y'\bar{\chi} \Phi^* N_R \\ & + \frac{\epsilon}{2} B^{\alpha\beta} Y_{\alpha\beta} + \mathcal{L}_\Phi + \mathcal{L}_\nu; \end{aligned} \tag{16}$$

where, $B^{\alpha\beta}$ ($Y_{\alpha\beta}$) denotes field strength tensors associated with $U(1)_D$ ($U(1)_Y$) respectively. Here, ϵ denotes the kinetic mixing between the two $U(1)$ sectors. The Lagrangian \mathcal{L}_Φ governing the singlet scalar Φ is expressed as:

$$\mathcal{L}_\Phi = (D_\mu \Phi)^\dagger (D^\mu \Phi) + m_\Phi^2 \Phi^\dagger \Phi - \lambda_\phi (\Phi^\dagger \Phi)^2 - \lambda_{\Phi H} (\Phi^\dagger \Phi) (H^\dagger H). \tag{17}$$

In this context, \mathcal{L}_ν represents the Lagrangian governing the UV-complete realizations discussed in subsequent sections. These realizations play crucial roles for achieving the necessary relic density of RHN. They also establishes the genesis of light neutrino masses. The singlet scalar field (Φ) serves two crucial functions. First, it attains a non-zero vacuum expectation value (VEV) $\langle \Phi \rangle = u$. This, in turn makes the gauge boson massive with $M_{Z'} = g_D u$. Second, it establishes a coupling between the RHN N_R and DM χ . This coupling plays the key role in generating the required SIDM relic, constituting a pivotal aspect of this scenario. Yukawa couplings connecting χ with N_R are assumed as identical ($y = y'$) and will be denoted as y for simplicity hereafter. It is crucial to emphasize that the coupling y is exceptionally small, fulfilling the relic density requirement and ensuring that DM predominantly exists as pure Dirac states. While there may be multiple generations of RHNs, for minimality, we specifically consider only the lightest among them to couple with DM.

4.2 SIDM phenomenology

The Lagrangian term $ig_D \bar{\chi} \gamma^\mu \chi Z'_\mu$ in Eqn. 16 facilitates the DM self scattering. The relevant Feynman graphs for self scattering is presented in the left segment of Fig. 3. Cross-section of self-interaction per unit SIDM mass with respect to the collision velocity (using Eqs. (9), (10), (11)) is fitted to available data from observations of different astrophysical objects [45, 89] in the right segment of Fig. 4. Different SIDM masses are depicted with color coded dashed lines. The fixed parameters are $M_{Z'} = 10 \text{ MeV}$ and $g_D = 0.1$. It is evident from this plot that, the model gives the desired velocity-dependent DM self-interaction.

Z' interacts with the SM Z boson via kinetic mixing (ϵ), creating an avenue for the direct detection of SIDM. The central diagram in Fig. 3 illustrates the Feynman diagram for direct search. Experiments dedicated to DM direct searches *e.g.*, CRESST-III [5] and XENON1T [4], constrains the kinetic mixing [20]. In the right segment of Fig. 4, the most rigorous restrictions by CRESST-III (XENON1T) for DM masses below (above) 10 GeV are portrayed against the SIDM-favored parameter space, assuming $g_D = 0.1$. The dashed black (purple) lines signify exclusion limits by the XENON1T (CRESST-III) for that particular value of ϵ . The region to the left of each contour is excluded for that particular value of kinetic mixing.

Regardless of whether it is thermal or non-thermal in origin, the ultimate relic density of DM remains relatively low, thanks to the substantial cross-section of DM annihilation ($\langle \sigma v \rangle \sim \frac{\pi \alpha_D^2}{m_\chi^2}$), driven by the large gauge coupling g_D . This is exemplified by Feynman graphs in the right segment of Fig. 3. The RHN (N_R) were in equilibrium with the thermal bath and subsequently freezes out. Frozen out N_R subsequently decays to a $\phi\chi$ pair at a later time. This late decay effectively rectifies the initially under-abundant relic. Given the potential mismatch between the masses of DM and N_R , thermal relic of N_R doesn't consistently reproduce the required DM relic density. Both freeze-out cross-section $\langle \sigma v \rangle_{F.O.}^{N_R}$ and decay width ($\Gamma_{N_R \rightarrow \phi\chi}$) of the RHN conspire to determine the correct relic

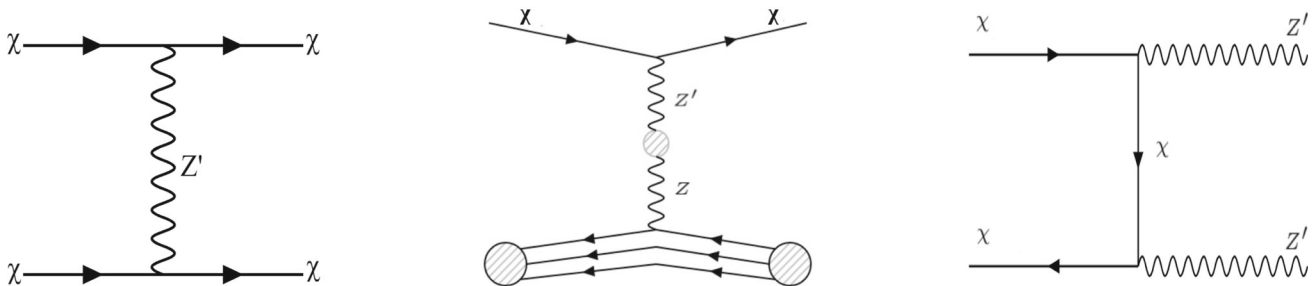


Fig. 3 Feynman graphs for DM self scattering (left), SIDM direct search (centre) and SIDM freeze-out (right)

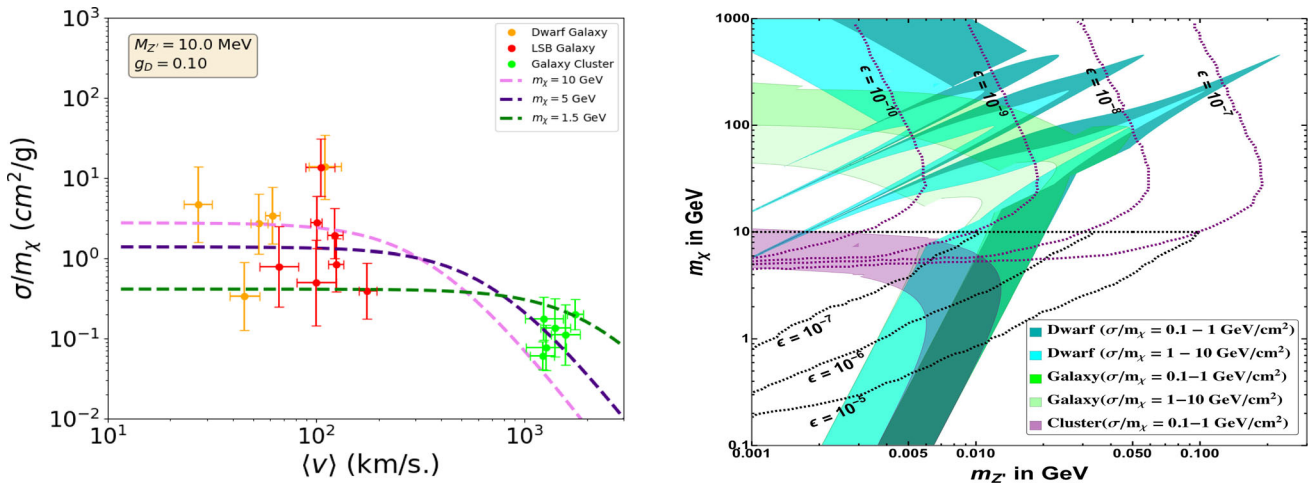


Fig. 4 [Right]: Parameter space aligned with sufficient self-interaction constrained by direct search. [Left]: Self scattering cross-section with respect to collision velocity

density of SIDM. For instance, if $\langle\sigma v\rangle_{F.O.}^{NR}$ is very small, we get a large freeze-out abundance of N_R . Therefore, $N_R \rightarrow \chi\phi$ decay must occur early enough for $\chi\chi \rightarrow Z'Z'$ annihilation to be active; otherwise, DM would be over-abundant. Conversely, if $\langle\sigma v\rangle_{F.O.}^{NR}$ matches the observed DM abundance for a specific DM mass m_χ , N_R must decay at a later epoch, rendering $\chi\chi \rightarrow Z'Z'$ nearly ineffective during the conversion of N_R abundance into DM abundance. If $\langle\sigma v\rangle_{F.O.}^{NR}$ assumes intermediate values between these two extremes, the observed relic density is achieved through an appropriate combination of $\langle\sigma v\rangle_{F.O.}^{NR}$ and $\Gamma_{N_R \rightarrow \phi\chi}$. As a result, a strong correlation exists between these two quantities to produce the observed DM relic density, as illustrated in the left segment in Fig. 5. Right segment in Fig. 5 further demonstrates the allowed region in the M_{N_R} vs $\langle\sigma v\rangle_{F.O.}^{NR}$ plane. The fixed parameters are $m_\chi = 1$ GeV and $y = 10^{-10}$. The behaviour is understood similar to the left panel figure, with the decay width being proportionate to mass.

The final parameter region in the $g_D - M_{Z'}$ plane is presented in the left segment of Fig. 6 where a benchmark of $m_\chi = 1$ GeV is considered. Upper left and lower right corners are considered unfavourable, due to either excessive or diminishing DM self-interactions. An intermediate band within these extremes remains viable. The upper left triangular region is partially disallowed by the CRESST-III [5] constraint, assuming $\epsilon = 10^{-10}$. Blue and red dotted lines represent future sensitivities of SuperCDMS [90] and DarkSide-LM [91]. Given that late DM annihilations lead to the copious production of Z' pairs, a conservative bound on the lifetime of Z' is imposed to ensure it is shorter than the typical epoch of BBN, preserving the BBN prediction regarding the abundance of light nuclei. In

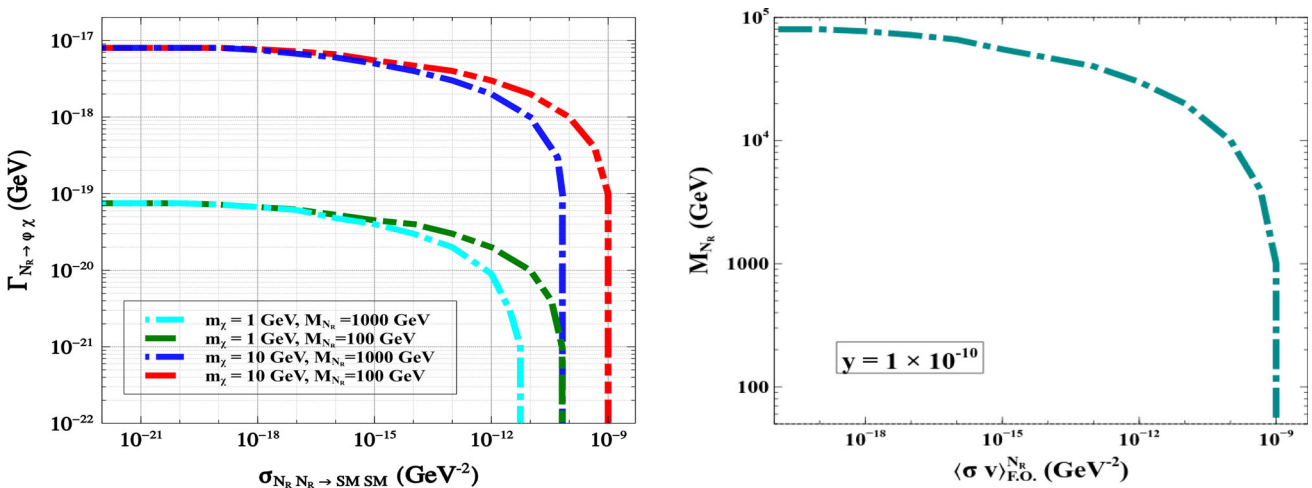


Fig. 5 [Left]: Contours of observed DM relic in $\langle\sigma v\rangle_{F.O.}^{NR}$ vs $\Gamma_{N_R \rightarrow \phi\chi}$ plane. [Right]: Range of RHN mass M_{N_R} for a fixed Yukawa coupling $y = 1 \times 10^{-10}$ that gives rise to required decay width

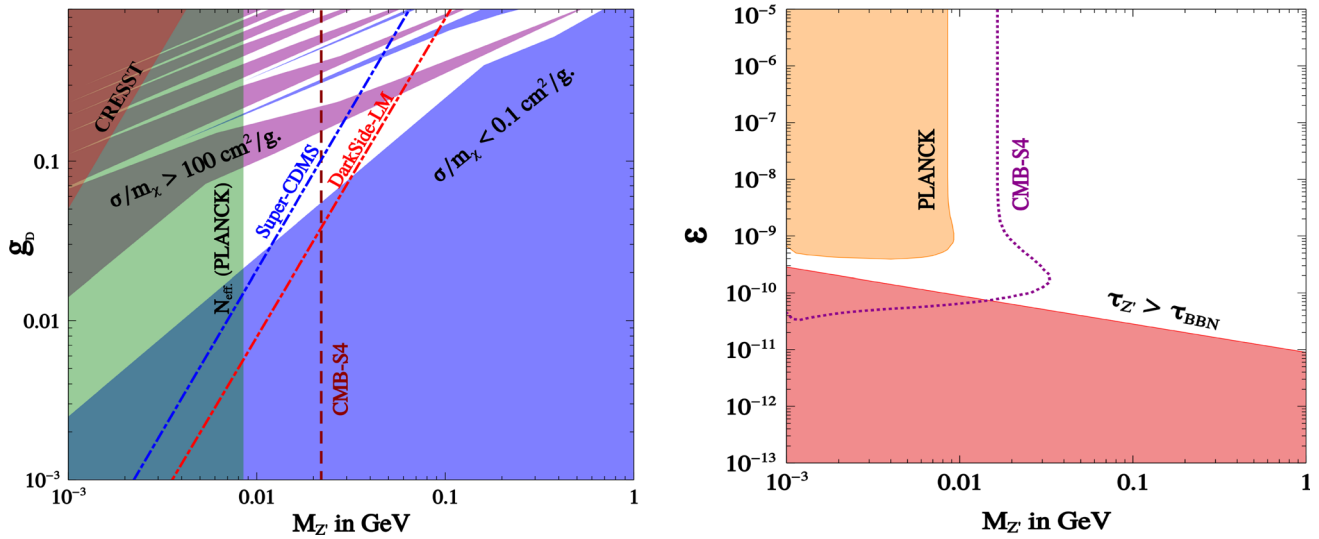


Fig. 6 [Left]: Parameter space in the plane of g_D vs $M_{Z'}$ for $m_\chi = 1$ GeV confronted with relevant constraints. [Right]: Parameter space in ϵ - $M_{Z'}$ plane

right segment of Fig. 6, ϵ is plotted against $M_{Z'}$, revealing that tiny kinetic mixing values (depicted in light red colour) are disfavored by this conservative limit. The benchmark values considered for ϵ in the preceding discussion inherently adhere to this limit. It is noteworthy that, thanks to a substantial gauge coupling, the decay $\phi \rightarrow Z'Z'$ occurs prior to BBN epoch. Z' bosons below a few MeVs are ruled out by limits on effective relativistic degrees of freedom [2, 75–77], illustrated by orange-shaded area, further constraining the available region in the ϵ vs $M_{Z'}$ plane. Additionally, the purple dotted line indicates the sensitivity of the parameter space relevant to CMB-S4 experiment in the future [76, 92].

4.3 UV-complete realization and connection to neutrino mass

4.3.1 Scotogenic realization

The scotogenic model [93] extends the Standard Model by incorporating three RHNs ($N_{1,2,3}$) and an additional doublet scalar η . All these fields carry odd charges under an imposed Z_2 gauge group, while SM fields are even. This setup allows coupling of SM lepton doublets to both η and RHNs, introducing a possibility to generate neutrino masses radiatively. The fermionic DM χ , being odd under Z_2 symmetry, couples with singlet scalar Φ via RHN portal. The BSM particle contents along with their charges is shown in Table 1.

The required Lagrangian consistent with imposed symmetries for generation of neutrino mass, encoded within the term \mathcal{L}_ν of the model Lagrangian Eqn. 16 is given by,

$$\mathcal{L}_\nu \supset Y_N \bar{L} \tilde{\eta} N_R + \text{h.c.}; \tag{18}$$

while the rest terms are the same as in Eq. 16. In this framework, the RHN portal SIDM scenario is realized by choosing N_1 to be lighter than η , preventing its decay into SM particles. Through fine-tuned coupling with SIDM, N_1 becomes long-lived. Although not the DM itself, N_1 freezes out yielding a relic that later transfers into SIDM relic. N_1 only has Yukawa interactions with the visible sectors. Sizable Yukawa values are needed for its desired thermal relic abundance. Unlike conventional low-scale seesaw models, the scotogenic model accommodates

Table 1 BSM particle content and charges under the chosen symmetry in the scotogenic realization

Fields		$SU(3)_c \otimes$	$SU(2)_L \otimes$	$SU(1)_Y$	$\otimes U(1)_D$	$\otimes Z_2$
Fermions	N_R	1	1	0	0	–
	χ	1	1	0	1	–
Scalars	η	1	2	1	0	–
	Φ	1	1	0	–1	+

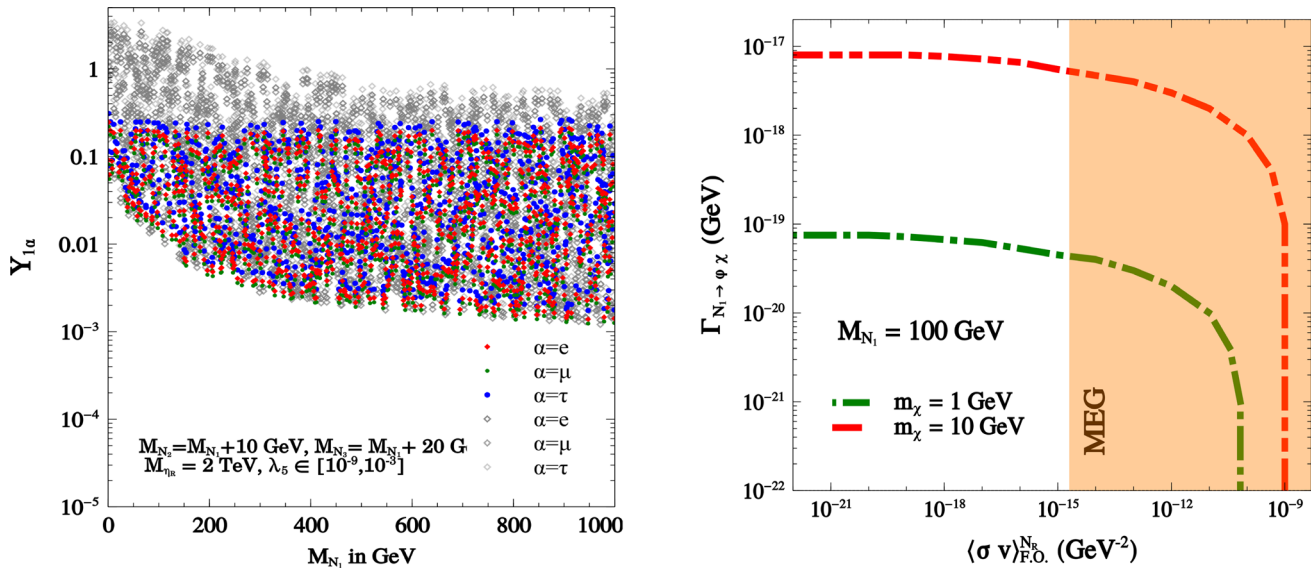


Fig. 7 [Left]: Parameter space within the scotogenic set-up, depicted in the plane of N_1 Yukawa coupling and its mass, in accordance with the relic abundance of SIDM. CLFV allowed regions are shown in colored dots (blue, red, green). Gray-boxed points, not overlapping with colored boxes are disallowed. [Right]: Contour lines outlining the correct SIDM relic in terms of cross-section and decay width. Disfavored region by MEG-CLFV bounds are shown in by orange shades

significant Yukawa couplings while complying with light neutrino mass constraints, thanks to loop suppression and scalar quartic coupling flexibility. The needed N_1 abundance relies on Yukawa couplings and mass splitting with other Z_2 odd particles. Dominant annihilation, co-annihilation or a combination of both mechanisms can achieve this.

Singlet RHNs elude collider constraints, but significant Yukawa couplings can pose challenges with CLFV. We show in the left segment of Fig. 7, the parameter space consistent with SIDM relic in scotogenic set-up in terms of N_1 Yukawa and its mass. In this figure, blue, cyan and pink dots are allowed from CLFV bounds. Grey boxes not overlapping with the coloured dots are disallowed. In right panel of Fig. 7, the contour lines depicting correct relic of DM are shown for $m_\chi = 1, 10$ GeV and $M_{N_1} = 100$ GeV in $\langle \sigma v \rangle_{F.O.}^{N_1}$ vs $\Gamma_{N_1 \rightarrow \phi \chi}$ plane. CLFV constraints from the MEG experiment [94] rules out the orange-shaded region. This region is characterized with large cross-sections *i.e.*, large N_1 Yukawa couplings, resulting in a very high CLFV rate, contrary to experimental limits. Clearly, the model parameters yielding the correct SIDM relic abundance remain testable in ongoing experiments.

4.3.2 Gauged B – L realization

Another intriguing UV completed RHN portal SIDM set-up is grounded in gauged B – L extension [95–100]. In this framework, alongside the SM and dark sectors, a singlet scalar ζ and three RHNs are introduced [20]. Incorporation of three RHNs with B – L charge -1 ensures an anomaly-free model. The BSM particle content along with their charges is shown in Table 2.

In light of this extension, the term \mathcal{L}_ν in the model Lagrangian Eq. 16 is given by,

$$\mathcal{L}_\nu \supset -\frac{1}{2} f \zeta \bar{N}_R^c N_R - Y_\nu \bar{L} \tilde{H} N_R + \text{h.c.}; \quad (19)$$

Table 2 Particle content and charges under imposed symmetries in gauged B – L set-up

Fields		$SU(3)_c \otimes$	$SU(2)_L \otimes$	$U(1)_Y$	$\otimes U(1)_{B-L}$	$\otimes U(1)_D$
Fermions	N_R	1	1	0	-1	0
	χ	1	1	0	0	1
Scalars	Φ	1	1	0	1	-1
	ζ	1	1	0	2	0

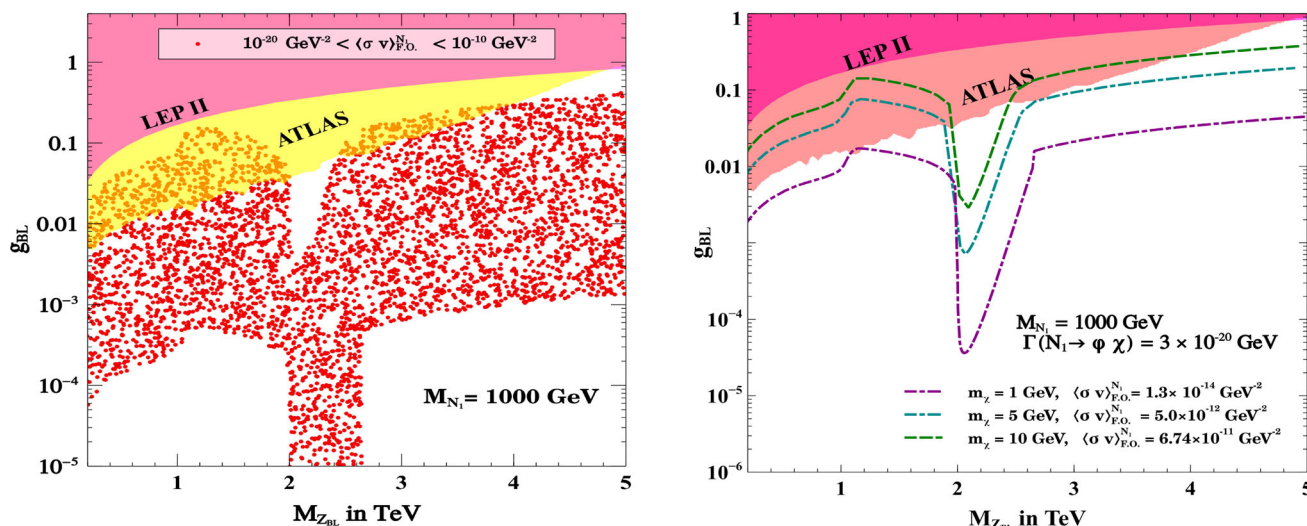


Fig. 8 [Left]: Parameter space within the B – L model that aligns with desired cross-section of the lightest RHN producing the required thermal abundance, which is subsequently transferred into the SIDM relic at a late epoch. [Right]: Contour lines in $M_{Z_{BL}}-g_{BL}$ plane representing the required cross-section $\langle\sigma v\rangle_{F.O.}^{N_1}$ capable of yielding the correct relic density for $m_\chi = 1, 5, 10$ GeV, with $M_{N_1} = 1000$ GeV and $\Gamma_{N_1\rightarrow\phi\chi} = 3 \times 10^{-20}$ GeV

other terms being same as in Eq. 16 except for the bare Majorana mass term $\frac{1}{2}M_{N_R}\overline{N^c}N_R$ which is not allowed due to imposed symmetries. However, the same can be generated by the scalar VEV. The scalar ζ acquires a non-zero VEV v_{BL} . This VEV spontaneously breaks the B – L symmetry. Besides, it generates RHN mass $M_{N_R} = fv_{BL}/\sqrt{2}$. Regarding the lightest right-handed neutrino (N_1) acting as a gateway to SIDM, notable differences exist between this set-up and the scotogenic model discussed earlier. In the gauged B – L model, N_1 connects with SM leptons via the SM Higgs (H), leading to its kinematic instability against decay into SM particles. Ensuring N_1 predominantly decays into SIDM at later times necessitates fine-tuned Yukawa couplings between N_1 and SM leptons, consequently yielding an exceedingly small lightest neutrino mass. An additional distinction is that, although N_1 might possess minute couplings to SM leptons, the potential for DM in this set-up to decay into SM neutrinos poses constraints from neutrino experiments. To be conservative, we consider the coupling of N_1 with SM leptons to be extremely small. The likelihood of probing this scenario in experiments targeting lepton flavor violation (LFV) is diminished compared to the scotogenic approach. However, it remains accessible via collider experiments.

RHNs are in equilibrium with the cosmic soup in the early universe, thanks to its gauged B – L and scalar portal interactions. Scalar portal interactions arise as ζ mixes with SM Higgs, which we omit in this study. We constrain gauge interactions solely from achieving a cross-section $\langle\sigma v\rangle_{N_1N_1\rightarrow SM, SM}$ that leads to suitable a freeze-out relic of N_1 . Gauge interactions of N_1 originate from kinetic terms: $\mathcal{L}_{kin} \supset i\overline{N}_R(\partial_\mu - ig_{BL}(Z_{BL})_\mu)N_R$.

For N_1 to achieve the desired freeze-out relic abundance, a substantial B – L coupling with the light Z_{BL} is necessary. This particular parameter space is subject to stringent constraints from collider experiments. Specifically, the investigation of resonances in high-mass dilepton production has imposed stringent constraints on the coupling of an additional gauge sector to SM fermions. The most recent constraints from ATLAS [101, 102] and CMS [103] experiments are considered to constrain the parameter space.

5 Singlet–doublet SIDM and radiative neutrino mass

In this work, we discuss another theoretical framework aimed at explaining SIDM together with the genesis of tiny neutrino mass in a singlet–doublet (SD) framework [21]. While fermionic singlet–doublet models are well-explored in the context of the WIMPs, this work takes a distinct approach. Rather than having a significant singlet–doublet mixing, as is typical in previous studies, here, we consider the mixing to be tiny. Hence, the DM candidate is predominantly the singlet fermion. Self scattering is facilitated with the help of an additional scalar field, which via its mixing with the SM Higgs, also offers a possibility of direct detection. Yukawa coupling of DM with the visible sector, which brings DM into thermal equilibrium, is also responsible for generating neutrino mass in a scotogenic setup [93]. However, due to the necessity of substantial self scattering, thermal relic of the singlet falls short to match the correct ballpark as it decays to light scalar very efficiently. Thanks to the tiny singlet–doublet

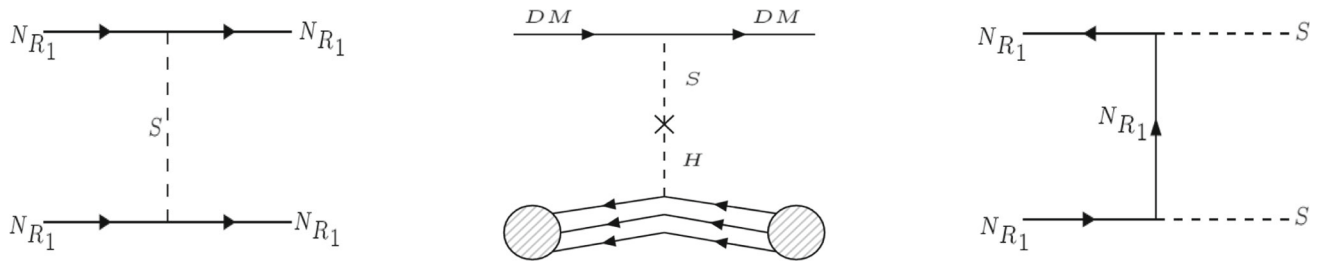


Fig. 9 Feynman graphs for DM self-interaction (left), SIDM direct search (centre) and SIDM freeze-out (right)

mixing, the doublet fermion becomes long-lived, enabling its late decay into the singlet. This process contributes to filling the relic abundance deficit.

5.1 The model setup

The SM particle content is augmented with a vector-like fermion doublet $\Psi^T = (\psi^0, \psi^-)$ and three gauge singlet RHNs N_{R_i} . Under an extra Z_2 symmetry, all these newly added fields are odd, whereas the SM fields remain even. A Z_2 -odd scalar doublet η is also added for generating neutrino mass radiatively. The model Lagrangian is given by,

$$\mathcal{L} = \mathcal{L}_{\text{SM}} + \bar{\Psi} [i\gamma^\mu(\partial_\mu - ig_2\frac{\sigma^a}{2}W_\mu^a - ig_1\frac{Y'}{2}B_\mu)] \Psi + \bar{N}_{R_i}(i\gamma^\mu\partial_\mu)N_{R_i} - M\bar{\Psi}\Psi - \frac{1}{2}M_{N_{R_i}}\bar{N}_{R_i}(N_{R_i})^c - y_i\bar{\Psi}\tilde{H}(N_{R_i} + (N_{R_i})^c) - Y_{\alpha i}\bar{L}\tilde{\eta}N_{R_i} - y_\Psi\bar{\Psi}\Psi S - y'_i\bar{N}_{R_i}(N_{R_i})^c S + \text{h.c.} + \mathcal{L}_{\text{scalar}}; \quad (20)$$

where $H(L)$ are Higgs (lepton) doublet of the SM. \mathcal{L}_{SM} stands for the SM Lagrangian, whereas $\mathcal{L}_{\text{scalar}}$ stands for the scalar part of the Lagrangian (see for details [21]). Due to tiny small singlet-doublet mixing ($y_i \sim 10^{-10}$), the lightest singlet N_{R_1} essentially acts as the SIDM candidate. The term $y'_1\bar{N}_{R_1}(N_{R_1})^c S$ of the Lagrangian is responsible for the self-interaction with the scalar S acting as the light mediator. Based on the model Lagrangian, the Feynman diagrams for DM self-interaction, direct-search and SIDM freeze-out are shown in Fig. 9.

5.2 SD-SIDM phenomenology

Doublet Ψ remains in equilibrium with the heat bath of the early cosmos via gauge interactions at temperatures above its mass scale. (N_{R_i}) too reach thermal equilibrium through $\Psi\Psi \xrightarrow{S} N_{R_i}N_{R_i}$, facilitated by the sizeable Yukawa $y'_i \sim 0.35$ essential for adequate self scattering. Yet, its freeze-out yields under-abundant relic up to DM mass of approximately 1 TeV, thanks to the substantial annihilation cross-section into light mediators. The longevity of the doublet Ψ is ensured by the tiny Yukawa coupling appearing in $y_i\bar{\Psi}\tilde{H}N_{R_i}$, enabling its late decay into the SM Higgs and N_{R_i} . As heavier singlets $N_{R_{2,3}}$ also eventually decay into N_{R_1} , they contribute to reinstating the correct DM relic abundance.

In the early cosmos, doublet number density diminishes through three primary processes: $\Psi\Psi \rightarrow S S$, $\Psi\Psi \rightarrow N_{R_i}N_{R_i}$, and $\Psi\Psi \rightarrow \text{SM SM}$. Assuming that the Yukawa coupling y_Ψ is significantly small, the process $\Psi\Psi \rightarrow \text{SM SM}$ predominantly determines the freeze-out density of Ψ .² Notably, the observed relic density is matched for $M_\Psi \approx 1000$ GeV only. Conversion of Ψ number density into DM number density transpires at a later epoch. To reproduce the correct DM relic, the following relation must be satisfied,

$$\Omega_{\text{DM}}h^2 = \left(\frac{M_{\text{DM}}}{M_\Psi}\right)\Omega_\Psi h^2. \quad (21)$$

Based on Eq.(21), the contour of the observed DM relic density in terms of M_Ψ and M_{DM} is presented in the right segment of Fig. 10. Notably, for light DM (below 10 GeV), a significantly heavy M_Ψ (above 150 TeV) is necessary to reproduce the correct relic. Conversely, as M_{DM} increases, M_Ψ decreases, ensuring adherence to Eq. (21).

By utilizing the cross-sections provided in Eqs. (9), (10), (11) along with imposition of constraints on σ/M_{DM} from astrophysical observations, we determine the parameter region for the model. This delineates the extent

²The inert doublet η also couples to N_{R_i} . Specific mass hierarchies of η and $N_{R_{2,3}}$ may impact their decays into each other. This in turn influences the DM relic density, since all particles odd under Z_2 eventually decays to DM.

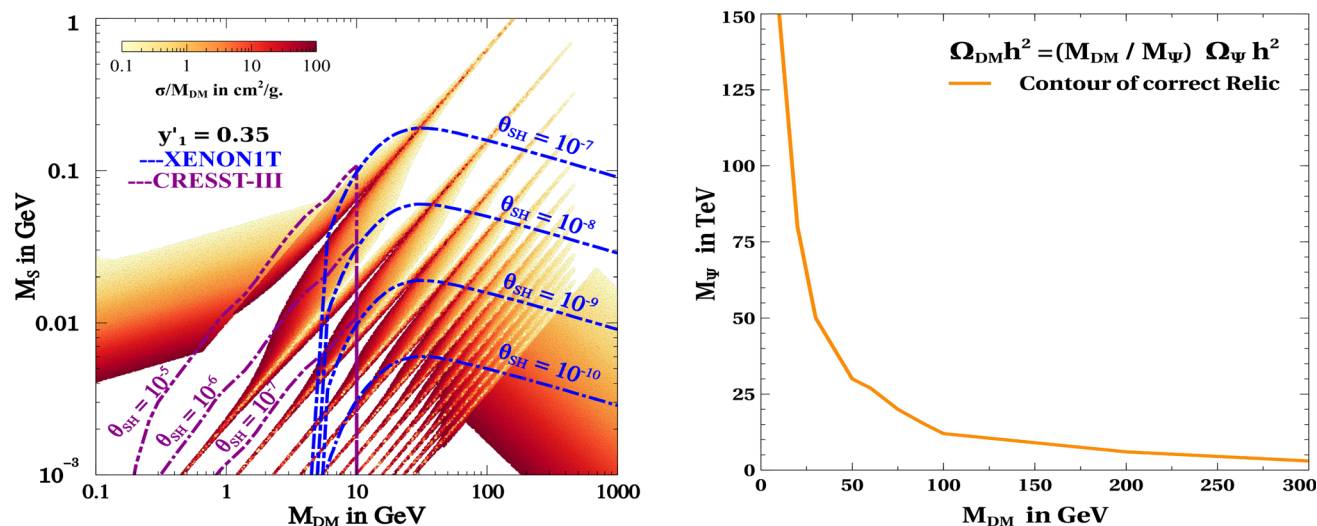


Fig. 10 [Left]: [Left]: The parameter space allowing for self-interaction constrained from direct search in the M_{DM} versus M_S plane. [Right]: Contour lines representing the observed relic density for N_{R_1}

of self-interaction in terms of M_{DM} and M_S as shown in the left segment of Fig. 10. The exclusion limits from the direct search experiments [4, 5] due to spin-independent elastic scattering via the $S - H$ mixing (θ_{SH}) are also projected against the SIDM parameter space. Region below each contour is disallowed for the specific θ_{SH} mentioned. It is worth mentioning that there exists an upper limit for θ_{SH} set by the process of invisible Higgs decay. Conversely, a lower limit for θ_{SH} can be derived from the condition that S decays prior to the onset of the BBN.

6 Conclusion

In this review, we explored the significance of SIDM in ameliorating the small-scale issues of Λ CDM as well as particle physics model building for SIDM. Models with a MeV scale mediator are well suited for realising the velocity-dependent self-interaction at the required ballpark. However, SIDM models with light mediators have difficulty explaining the observed DM abundance, as the former annihilates too efficiently into the latter. In addition, masses and couplings are also stringently constrained by direct search experiments, astrophysical observations and BBN. Here, we have discussed two specific SIDM set-ups incorporating tiny neutrino masses [20, 21]. The first setup involves a RHN portal that offers a non-thermal way to adjust for the relic deficit through late time RHN decay. This connects to neutrino mass and is realized in two UV complete ways: the scotogenic and gauged $B - L$ frameworks. The second setup features a singlet–doublet model with self-interactions being mediated by a light scalar. Due to its minute mixing with the singlet, the doublet becomes long-lived and contribute non-thermally to the singlet relic abundance. In both approaches, the allowed parameter space has been confronted with relevant phenomenological and experimental constraints. SIDM is an active domain and there are several other interesting models that have been proposed. While various model realizations may yield similar outcomes, the allure lies in models that extend beyond mere SIDM considerations. The appeal is heightened when a proposed model can concurrently address broader questions, such as neutrino mass or the Baryon asymmetry. Furthermore, the evaluation of detection prospects adds an intriguing dimension, especially in the context of collider and CLFV experiments or dark photon searches. Specifically, in the RHN portal scenario, the scotogenic model remains predictive in experiments targeting charged lepton flavor violation, while the $B - L$ setup retains predictiveness in collider experiments. Similarly, the singlet–doublet scenario may also yield tantalizing signals at colliders. This review encourages a holistic approach, advocating for SIDM models that not only offer a comprehensive explanation for their specific phenomena but also contribute to resolving broader challenges in the realm of particle physics and cosmology. In the upcoming decade, several near-future experiments with better resolution and strong statistics will shed light on observations relevant to SIDM.

Acknowledgements SM acknowledges the support from National Research Foundation of Korea grant 2022R1A2C1005050. The authors gratefully acknowledge Debasish Borah and Narendra Sahu for their extensive collaboration on this subject.

Data availability statement No data associated in the manuscript.

References

1. G. Hinshaw et al., WMAP. *Astrophys. J. Suppl.* **208**, 19 (2013). [arXiv:1212.5226](#)
2. N. Aghanim et al. (Planck), *Astron. Astrophys.* **641**, A6 (2020), [Erratum: *Astron. Astrophys.* 652, C4 (2021)], [arXiv:1807.06209](#)
3. J. Aalbers et al. (LZ), *Phys. Rev. Lett.* **131**, 041002 (2023), [arXiv:2207.03764](#)
4. E. Aprile et al. (XENON), *Phys. Rev. Lett.* **121**, 111302 (2018), [arXiv:1805.12562](#)
5. A. Abdelhameed et al. (CRESST), *Phys. Rev. D* **100**, 102002 (2019), [arXiv:1904.00498](#)
6. J.F. Navarro, C.S. Frenk, S.D.M. White, *Astrophys. J.* **490**, 493 (1997). [arXiv:astro-ph/9611107](#)
7. R.H. Wechsler, J.S. Bullock, J.R. Primack, A.V. Kravtsov, A. Dekel, *Astrophys. J.* **568**, 52 (2002). [arXiv:astro-ph/0108151](#)
8. W.J.G. de Blok, *Adv. Astronomy* **2010**, 789293 (2010). [arXiv:0910.3538](#)
9. J.S. Bullock, M. Boylan-Kolchin, *Ann. Rev. Astron. Astrophys.* **55**, 343 (2017). [arXiv:1707.04256](#)
10. B. Moore, S. Ghigna, F. Governato, G. Lake, T.R. Quinn, J. Stadel, P. Tozzi, *Astrophys. J. Lett.* **524**, L19 (1999). [arXiv:astro-ph/9907411](#)
11. A.A. Klypin, A.V. Kravtsov, O. Valenzuela, F. Prada, *Astrophys. J.* **522**, 82 (1999). [arXiv:astro-ph/9901240](#)
12. M. Boylan-Kolchin, J. S. Bullock, and M. Kaplinghat, *Monthly Notices of the Royal Astronomical Society: Letters* **415**, L40-L44 (2011b), ISSN 1745-3925
13. M. Boylan-Kolchin, J. S. Bullock, and M. Kaplinghat, *Monthly Notices of the Royal Astronomical Society* **422**, 1203-1218 (2012b), ISSN 0035-8711
14. D.N. Spergel, P.J. Steinhardt, *Phys. Rev. Lett.* **84**, 3760 (2000). [arXiv:astro-ph/9909386](#)
15. E.D. Carlson, M.E. Machacek, L.J. Hall, *Astrophys. J.* **398**, 43 (1992)
16. A.A. de Laix, R.J. Scherrer, R.K. Schaefer, *Astrophys. J.* **452**, 495 (1995). [arXiv:astro-ph/9502087](#)
17. S. W. Randall, M. Markevitch, D. Clowe, A. H. Gonzalez, and M. Bradač, *The Astrophysical Journal* **679**, 1173-1180 (2008), ISSN 1538-4357
18. S. Tulin, H.-B. Yu, *Phys. Rept.* **730**, 1 (2018). [arXiv:1705.02358](#)
19. S. Tulin, H.-B. Yu, K.M. Zurek, *Phys. Rev. D* **87**, 115007 (2013). [arXiv:1302.3898](#)
20. D. Borah, M. Dutta, S. Mahapatra, N. Sahu, *Phys. Rev. D* **105**, 015004 (2022). [arXiv:2110.00021](#)
21. D. Borah, M. Dutta, S. Mahapatra, N. Sahu, *Phys. Rev. D* **105**, 075019 (2022). [arXiv:2112.06847](#)
22. S.-H. Oh, W. J. G. de Blok, E. Brinks, F. Walter, and R. C. Kennicutt, *The Astronomical Journal* **141**, 193 (2011), ISSN 1538-3881
23. M.R. Buckley, P.J. Fox, *Phys. Rev. D* **81**, 083522 (2010). [arXiv:0911.3898](#)
24. J.L. Feng, M. Kaplinghat, H.-B. Yu, *Phys. Rev. Lett.* **104**, 151301 (2010). [arXiv:0911.0422](#)
25. J.L. Feng, M. Kaplinghat, H. Tu, H.-B. Yu, *JCAP* **07**, 004 (2009). [arXiv:0905.3039](#)
26. A. Loeb, N. Weiner, *Phys. Rev. Lett.* **106**, 171302 (2011). [arXiv:1011.6374](#)
27. J. Zavala, M. Vogelsberger, M.G. Walker, *Mon. Not. Roy. Astron. Soc.* **431**, L20 (2013). [arXiv:1211.6426](#)
28. M. Vogelsberger, J. Zavala, A. Loeb, *Mon. Not. Roy. Astron. Soc.* **423**, 3740 (2012). [arXiv:1201.5892](#)
29. J.F. Navarro, C.S. Frenk, S.D.M. White, *Astrophys. J.* **462**, 563 (1996). [arXiv:astro-ph/9508025](#)
30. J. Dubinski, R.G. Carlberg, *Astrophys. J.* **378**, 496 (1991)
31. B. Moore, *Nature* **370**, 629 (1994)
32. B. Moore, T.R. Quinn, F. Governato, J. Stadel, G. Lake, *Mon. Not. Roy. Astron. Soc.* **310**, 1147 (1999). [arXiv:astro-ph/9903164](#)
33. A. Burkert, *Astrophys. J. Lett.* **447**, L25 (1995). [arXiv:astro-ph/9504041](#)
34. S.S. McGaugh, W.J.G. de Blok, *Astrophys. J.* **499**, 41 (1998). [arXiv:astro-ph/9801123](#)
35. S. Côté, C. Carignan, K.C. Freeman, *Astron. J.* **120**, 3027 (2000)
36. J.D. Simon, A.D. Bolatto, A. Leroy, L. Blitz, *A.S.P. Conf. Ser.* **327**, 18 (2004). [arXiv:astro-ph/0310193](#)
37. A. Borriello, P. Salucci, *Mon. Not. Roy. Astron. Soc.* **323**, 285 (2001). [arXiv:astro-ph/0001082](#)
38. W.J.G. de Blok, S.S. McGaugh, V.C. Rubin, *Astron. J.* **122**, 2396 (2001)
39. W.J.G. de Blok, S.S. McGaugh, A. Bosma, V.C. Rubin, *Astrophys. J. Lett.* **552**, L23 (2001). [arXiv:astro-ph/0103102](#)
40. D. Marchesini, E. D'Onghia, G. Chincarini, C. Firmani, P. Conconi, E. Molinari, A. Zacchei, *Astrophys. J.* **575**, 801 (2002). [arXiv:astro-ph/0202075](#)
41. G. Gentile, A. Burkert, P. Salucci, U. Klein, F. Walter, *Astrophys. J. Lett.* **634**, L145 (2005). [arXiv:astro-ph/0506538](#)
42. R. Kuzio de Naray, S.S. McGaugh, W.J.G. de Blok, A. Bosma, *Astrophys. J. Suppl.* **165**, 461 (2006). [arXiv:astro-ph/0604576](#)
43. R. Kuzio de Naray, S.S. McGaugh, W.J.G. de Blok, *Astrophys. J.* **676**, 920 (2008). [arXiv:0712.0860](#)
44. P. Salucci, A. Lapi, C. Tonini, G. Gentile, I. Yegorova, U. Klein, *Mon. Not. Roy. Astron. Soc.* **378**, 41 (2007). [arXiv:astro-ph/0703115](#)
45. M. Kaplinghat, S. Tulin, H.-B. Yu, *Phys. Rev. Lett.* **116**, 041302 (2016). [arXiv:1508.03339](#)
46. A. Kamada, M. Kaplinghat, A. B. Pace, and H.-B. Yu, *Physical Review Letters* **119** (2017), ISSN 1079-7114
47. J. Miralda-Escude, *The Astrophysical Journal* **564**, 60-64 (2002), ISSN 1538-4357

48. M. Meneghetti, N. Yoshida, M. Bartelmann, L. Moscardini, V. Springel, G. Tormen, and S. D. M. White, *Mon. Notices R. Astron. Soc.* **325**, 435-442 (2001), ISSN 1365-2966
49. F. Kahlhoefer, K. Schmidt-Hoberg, M. T. Frandsen, and S. Sarkar, *Mon. Not. R. Astron. Soc.* **437**, 2865-2881 (2013), ISSN 1365-2966
50. A. Robertson, R. Massey, and V. Eke, *Mon. Not. R. Astron. Soc.* **465**, 569-587 (2016), ISSN 1365-2966
51. S. Y. Kim, A. H. G. Peter, and D. Wittman, *Mon. Not. R. Astron. Soc.* **469**, 1414-1444 (2017a), ISSN 1365-2966
52. S. Y. Kim, A. H. G. Peter, and D. Wittman, *Mon. Not. R. Astron. Soc.* **469**, 1414-1444 (2017b), ISSN 1365-2966
53. M. Rocha, A.H.G. Peter, J.S. Bullock, M. Kaplinghat, S. Garrison-Kimmel, J. Onorbe, L.A. Moustakas, *Mon. Not. Roy. Astron. Soc.* **430**, 81 (2013). [arXiv:1208.3025](#)
54. A.H.G. Peter, M. Rocha, J.S. Bullock, M. Kaplinghat, *Mon. Not. Roy. Astron. Soc.* **430**, 105 (2013). [arXiv:1208.3026](#)
55. O.D. Elbert, J.S. Bullock, S. Garrison-Kimmel, M. Rocha, J. Oñorbe, A.H.G. Peter, *Mon. Not. Roy. Astron. Soc.* **453**, 29 (2015). [arXiv:1412.1477](#)
56. M. C. Bento, O. Bertolami, R. Rosenfeld, and L. Teodoro, *Phys. Rev. D* **62** (2000), ISSN 1089-4918
57. J. McDonald, *Phys. Rev. Lett.* **88**, 091304 (2002). [arXiv:hep-ph/0106249](#)
58. L. Ackerman, M. R. Buckley, S. M. Carroll, and M. Kamionkowski, *Phys. Rev. D* **79** (2009), ISSN 1550-2368
59. S. Tulin, H.-B. Yu, K.M. Zurek, *Phys. Rev. Lett.* **110**, 111301 (2013). [arXiv:1210.0900](#)
60. Y. Hochberg, E. Kuflik, T. Volansky, J.G. Wacker, *Phys. Rev. Lett.* **113**, 171301 (2014)
61. Yonit Hochberg, Eric Kuflik, Hitoshi Murayama, Tomer Volansky, Jay G. Wacker, *Phys. Rev. Lett.* **115**, 021301 (2015)
62. Ayuki Kamada, Masaki Yamada, Tsutomu T. Yanagida, *Phys. Rev. D* **102**, 075001 (2020)
63. Ayuki Kamada, Hee Jung Kim, Hyungjin Kim, Toyokazu Sekiguchi. *Phys. Rev. Lett.* **120**, 131802 (2018)
64. Ayuki Kamada, Hee Jung Kim, Hyungjin Kim. *Phys. Rev. D* **98**, 023509 (2018)
65. Xiaoyong Chu, Camilo Garcia-Cely, *JCAP* **07**, 013 (2018)
66. M. Ibe and H.-B. Yu, *Physics Letters B* **692**, 70-73 (2010), ISSN 0370-2693
67. T. Bringmann, F. Kahlhoefer, K. Schmidt-Hoberg, P. Walia, *Phys. Rev. Lett.* **118**, 141802 (2017). [arXiv:1612.00845](#)
68. L.G. van den Aarssen, T. Bringmann, C. Pfrommer, *Phys. Rev. Lett.* **109**, 231301 (2012). [arXiv:1205.5809](#)
69. K. Schutz, T.R. Slatyer, *JCAP* **01**, 021 (2015). [arXiv:1409.2867](#)
70. P. Agrawal, F.-Y. Cyr-Racine, L. Randall, and J. Scholtz, *J. Cosmol. Astroparticle Phys.* **2017**, 022-022 (2017), ISSN 1475-7516
71. S.A. Khrapak, A.V. Ivlev, G.E. Morfill, S.K. Zhdanov, *Phys. Rev. Lett.* **90**, 225002 (2003)
72. S.A. Khrapak, A.V. Ivlev, G.E. Morfill, *Phys. Rev. E* **70**, 056405 (2004)
73. M. Kaplinghat, S. Tulin, H.-B. Yu, *Phys. Rev. D* **89**, 035009 (2014). [arXiv:1310.7945](#)
74. E. Del Nobile, M. Kaplinghat, H.-B. Yu, *JCAP* **10**, 055 (2015). [arXiv:1507.04007](#)
75. A. Kamada, K. Kaneta, K. Yanagi, H.-B. Yu, *JHEP* **06**, 117 (2018). [arXiv:1805.00651](#)
76. M. Ibe, S. Kobayashi, Y. Nakayama, S. Shirai, *JHEP* **04**, 009 (2020). [arXiv:1912.12152](#)
77. M. Escudero, D. Hooper, G. Krnjaic, M. Pierre, *JHEP* **03**, 071 (2019). [arXiv:1901.02010](#)
78. C. Kouvaris, I.M. Shoemaker, K. Tuominen, *Phys. Rev. D* **91**, 043519 (2015). [arXiv:1411.3730](#)
79. N. Bernal, X. Chu, C. Garcia-Cely, T. Hambye, B. Zaldivar, *JCAP* **03**, 018 (2016). [arXiv:1510.08063](#)
80. K. Kainulainen, K. Tuominen, and V. Vaskonen, *Phys. Rev. D* **93**, 015016 (2016), [Erratum: *Phys.Rev.D* 95, 079901 (2017)], [arXiv:1507.04931](#)
81. T. Hambye, L. Vanderheyden, *JCAP* **05**, 001 (2020). [arXiv:1912.11708](#)
82. M. Cirelli, P. Panci, K. Petraki, F. Sala, M. Taoso, *JCAP* **05**, 036 (2017). [arXiv:1612.07295](#)
83. F. Kahlhoefer, K. Schmidt-Hoberg, S. Wild, *JCAP* **08**, 003 (2017). [arXiv:1704.02149](#)
84. M. Dutta, N. Narendra, N. Sahu, S. Shil, *Phys. Rev. D* **106**, 095017 (2022). [arXiv:2202.04704](#)
85. M. Dutta, S. Mahapatra, D. Borah, N. Sahu, *Phys. Rev. D* **103**, 095018 (2021). [arXiv:2101.06472](#)
86. D. Borah, M. Dutta, S. Mahapatra, N. Sahu, *Nucl. Phys. B* **979**, 115787 (2022). [arXiv:2107.13176](#)
87. D. Borah, A. Dasgupta, S. Mahapatra, N. Sahu, *Phys. Rev. D* **106**, 095028 (2022). [arXiv:2112.14786](#)
88. D. Borah, S. Mahapatra, and N. Sahu (2022e), [arXiv:2211.15703](#)
89. A. Kamada, H.J. Kim, T. Kuwahara, *JHEP* **20**, 202 (2020). [arXiv:2007.15522](#)
90. R. Agnese et al. (SuperCDMS), *Phys. Rev. D* **95**, 082002 (2017), [arXiv:1610.00006](#)
91. P. Agnes et al. (DarkSide), *Phys. Rev. Lett.* **121**, 081307 (2018), [arXiv:1802.06994](#)
92. K. N. Abazajian et al. (CMB-S4) (2016), [arXiv:1610.02743](#)
93. E. Ma, *Phys. Rev. D* **73**, 077301 (2006). [arXiv:hep-ph/0601225](#)
94. A. M. Baldini et al. (MEG), *Eur. Phys. J. C* **76**, 434 (2016), [arXiv:1605.05081](#)
95. A. Davidson, *Phys. Rev. D* **20**, 776 (1979)
96. R. N. Mohapatra and R. E. Marshak, *Phys. Rev. Lett.* **44**, 1316 (1980), [Erratum: *Phys. Rev. Lett.* 44,1643(1980)]
97. R.E. Marshak, R.N. Mohapatra, *Phys. Lett.* **91B**, 222 (1980)
98. A. Masiero, J.F. Nieves, T. Yanagida, *Phys. Lett.* **116B**, 11 (1982)
99. R.N. Mohapatra, G. Senjanovic, *Phys. Rev. D* **27**, 254 (1983)
100. W. Buchmuller, C. Greub, P. Minkowski, *Phys. Lett. B* **267**, 395 (1991)
101. M. Aaboud et al. (ATLAS) (2017), [arXiv:1707.02424](#)
102. G. Aad et al. (ATLAS), *Phys. Lett.* **B796**, 68 (2019), [arXiv:1903.06248](#)
103. A. M. Sirunyan et al. (CMS), *JHEP* **06**, 120 (2018), [arXiv:1803.06292](#)

Springer Nature or its licensor (e.g. a society or other partner) holds exclusive rights to this article under a publishing agreement with the author(s) or other rightsholder(s); author self-archiving of the accepted manuscript version of this article is solely governed by the terms of such publishing agreement and applicable law.